Proceedings of the 21st ICSMGE, Vienna, Austria, 14 – 19 June 2026. Pistrol, Adam & Schweiger (eds.)
Published by: ÖGG, Austrian Society for Geomechanics, Salzburg, Austria, ISBN 978-3-9503898-4-5
https://doi.org/10.53243/ICSMGE2026-744

Automated Calibration of Advanced Constitutive Models for Cyclic Liquefaction

Sheng Zeng
Department of Civil Engineering, University of British Columbia, Vancouver, BC, Canada

Jan Machaček, Hauke Zachert
Institute of Geotechnics, Technical University of Darmstadt, Germany

Mahdi Taiebat
Department of Civil Engineering, University of British Columbia, Vancouver, BC, Canada, mtaiebat@civil.ubc.ca

ABSTRACT: Reliable geotechnical predictions for cyclic liquefaction problems require selecting constitutive models with capabilities relevant to the problem and ensuring their effective calibration; the latter remains time-consuming and expertise-intensive, thereby hindering the practical adoption of advanced models. This study presents an automatic calibration (AC) tool designed to streamline parameter identification for advanced constitutive models, accommodating a wide range of laboratory test data. Using the proposed tool, the SANISAND-MSf model parameters were calibrated for Ottawa-F65 sand based on extensive element-level test data. The AC follows a two-stage approach: first, optimizing the base parameters governing monotonic response using monotonic test data; second, refining these and additional cyclic-specific parameters using both monotonic and cyclic data. Critical state parameters remain fixed throughout, while elasticity constants are fixed in the second stage, all within predefined bounds to ensure reasonable results. The AC parameters were assessed through simulations of centrifuge tests of a submerged sand slope subjected to base excitations. Simulation results showed excellent agreement with experimental data, confirming the tool's robustness, accuracy, and reproducibility. This work highlights that the expertise and time required to calibrate advanced constitutive models can be significantly reduced while maintaining high predictive accuracy, thereby advancing their broader adoption in geotechnical engineering practice.

KEYWORDS: Automatic calibration tool, cyclic liquefaction, sand plasticity model.

1 INTRODUCTION

Accurate simulation of soil behavior under undrained cyclic loading relies not only on the constitutive model's predictive capability but also on effective parameter calibration, which is often time-consuming and demands expert knowledge, particularly for advanced models such as bounding surface plasticity, nested plasticity, and hypoplasticity. To address these challenges, automatic calibration strategies, such as numgeo-ACT (Machaček et al., 2022, 2023; Brosz et al., 2023), have been developed, framing parameter calibration as an optimization problem that minimizes the discrepancy between model predictions and experimental data. This study focuses on two key questions: (i) Can AC optimization converge effectively for cyclic loading data, which is more complex than monotonic loading? and (ii) If so, do the optimized parameters yield robust and comparable predictions for boundary value problems (BVPs) compared to expert manual calibration?

To address these questions, this paper extends numgeo-ACT to calibrate an advanced constitutive model under cyclic loading, surpassing the capabilities of existing tools. Its performance is demonstrated using the SANISAND-MSf model (Yang et al., 2022), a critical state bounding surface plasticity model with memory surface (M) and semifluidized states (Sf) specifically targeting adequate modeling of cyclic liquefaction triggering and post-liquefaction cyclic shear strain accumulation. Calibration and validation are conducted using data from the Liquefaction Experiments and Analysis Projects (LEAP). The study includes both element tests from LEAP-2020 (ElGhoraiby and Manzari, 2021) and LEAP-2022 (Lbibb and Manzari, 2022), and a centrifuge test of a liquefiable sand slope subjected to base shaking from LEAP-2017 (Kutter et al., 2020). The tool's effectiveness is evaluated through these simulations, demonstrating that automatically calibrated parameters can yield reliable model predictions at both the element level and in BVPs. The results provide insight into the practical applicability of automatically calibrated parameters for geotechnical engineers and researchers. An extended version of this work, including additional analyses and discussions, is presented in Machaček et al. (2025a).

2 AUTOMATIC CALIBRATION TOOL

The numgeo-ACT is a Python-based toolset for automatic calibration of soil constitutive models using various laboratory tests, including oedometer, drained/undrained triaxial, and simple shear tests under both monotonic and cyclic loading. It employs the freely available finite element program numgeo (www.numgeo.de) to perform single-element simulations. The ACT workflow is illustrated in Figure 1 and described below.

Calibration begins with simulations using an initial parameter set, followed by comparison with experimental data.

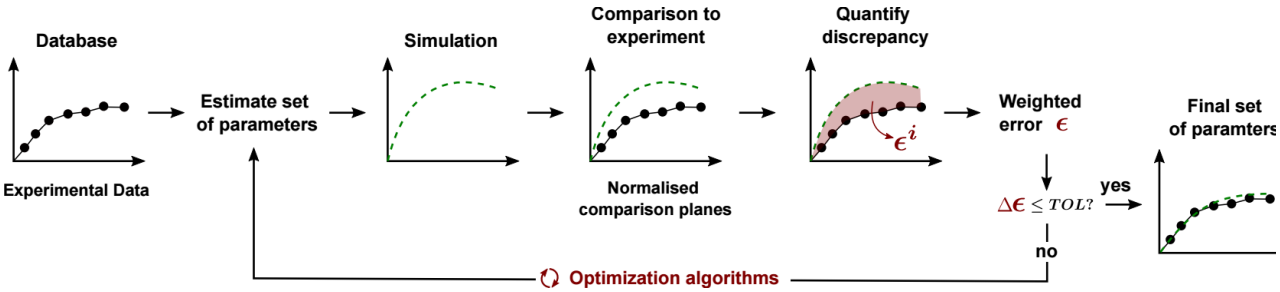

Figure 1. General workflow of numgeo-ACT.

The discrepancy is quantified using the discrete Fréchet distance, applied in scaled stress–strain space to ensure equal weighting of all variables. Accordingly, a weighted error ϵ, named the cost function, is computed across all tests and used to evaluate the performance of parameter sets. Model parameters are then iteratively refined within user-defined bounds using a fast and robust optimization algorithm, DEEM (differential evolution with elitism and multi-populations, Machaček et al., 2025b), with a population size of 100 candidate solutions, resulting in 100 different parameter sets tested per iteration. The optimization process stops when either the maximum 200 iterations is reached, or the change in error $\Delta\epsilon$ over 50 iterations drops below a tolerance of 10^{-6}. These stopping criteria are user-adjustable.

3 AUTOMATIC CALIBRATION FOR OTTAWA-F65

To demonstrate the effectiveness of the ACT, the SANISAND-MSf model is calibrated using a comprehensive series of consolidated drained monotonic triaxial (CD) and cyclic direct simple shear (CDSS) tests on Ottawa-F65 sand from the LEAP project.

3.1 *Experimental database*

Ottawa-F65 is a poorly graded clean sand composed of approximately 99% subrounded silica and about 1% fines, supplied by US Silica. Its maximum and minimum densities are 1.757 and 1.491 t/m^3, respectively, with a specific gravity of 2.65 and a hydraulic conductivity ranging from 1.0×10^{-4} m/s to 1.6×10^{-4} m/s (Kutter et al., 2020). Several monotonic triaxial tests were provided by ElGhoraiby et al. (2020), including 20 consolidated drained (CD) and 24 undrained (CU) tests that were used to determine the critical state line. Additionally, 65 CDSS tests were reported, covering a wide range of initial void ratios (e_{ini}), vertical stresses ($\sigma_{\mathrm{v,ini}}$), static shear stresses (τ_{ini}), and cyclic stress ratios (CSR) (ElGhoraiby and Manzari, 2021; Lbibb and Manzari, 2022).

For parameter optimization by the ACT, four CD tests were used with e_{ini} between 0.575 and 0.726, and the initial mean effective stress $p_{\mathrm{ini}} = 100$ kPa. Other CD tests in the above dataset were not reported with complete stress-strain records and, therefore, were excluded from the optimization process in this study. In addition, only 18 out of 65 CDSS tests were selected to strike a balance between coverage of the initial states and loading conditions, as listed in Table 1, and the computational cost. All CDSS tests started from K_0 stress conditions, while those with non-zero τ_{ini} were first sheared in drained conditions until the target τ_{ini} was reached. Subsequently, samples were subjected to constant volume cyclic loading with CSR values ranging from 0.13 to 0.24.

Table 1. Subset of CDSS tests on Ottawa-F65 sand used for automatic calibration.

T#	e_{ini}	$\sigma_{\mathrm{v,ini}}$ (kPa)	τ_{ini} (kPa)	CSR	T#	e_{ini}	$\sigma_{\mathrm{v,ini}}$ (kPa)	τ_{ini} (kPa)	CSR
1	0.598	100	0	0.13	10	0.601	40	10	0.2
2	0.631	40	0	0.15	11	0.601	40	10	0.23
3	0.600	40	0	0.15	12	0.601	40	10	0.25
4	0.600	40	0	0.19	13	0.601	40	15	0.25
5	0.601	40	0	0.21	14	0.601	40	15	0.27
6	0.576	40	0	0.16	15	0.601	40	15	0.30
7	0.600	100	0	0.17	16	0.601	40	15	0.32
8	0.600	100	0	0.19	17	0.601	100	30	0.25
9	0.600	100	0	0.21	18	0.600	100	40	0.25

3.2 *Soil constitutive model and optimization constraints*

The SANISAND-MSf (S-MSf) model developed by Yang et al. (2022) is adopted in this study. It builds on the two-surface DM04 model by Dafalias and Manzari (2004), retaining key features such as stress ratio control, critical state compatibility, and bounding surface plasticity. The model incorporates a Drucker-Prager yield surface with kinematic hardening centered at a back-stress ratio and with a small opening m, along with three Lode angle-dependent surfaces (critical state, bounding, and dilatancy), all formulated in multiaxial stress space. Governed by state variables, these surfaces are designed to allow a unified set of parameters to represent density- and pressure-dependent behaviors, including hardening/softening and contraction/dilation. Two additional features, a memory surface (M) and a semifluidized state (Sf), adopted and modified from Corti et al. (2016), Liu et al. (2019), and Barrero et al (2020), are designed to improve the S-MSf model's regulation of cyclic excess pore pressure buildup and cyclic shear strain accumulation under cyclic shearing, enabling it to capture both cyclic liquefaction resistance curves and post-liquefaction shear behavior across varying CSRs. The model is implemented in OpenSees and numgeo (following Ghofrani, 2018) using a modified Euler explicit integration scheme with automatic substepping and error control (Sloan et al., 2001), as well as a treatment for low mean effective stresses.

In parameter optimization for advanced constitutive models, constraining the search space is essential to avoid nonphysical values and numerical instability. The bounds of each parameter used in this study are summarized in Table 2, based on previous experience with manual calibrations of SANISAND models for various materials. In the second calibration stage, upper bounds were set at roughly twice the calibrated values from the first stage, while lower bounds were relaxed to allow deactivation of certain model ingredients if

Table 2. Model parameters of the SANISAND-MSf model for Ottawa-F65 sand, reference manual calibration (Zeng et al., 2024), and respective bounds for the automatic calibration.

Model parameter	Symbol	Reference	Bounds
Elasticity	G_0	125	(50, 200)
	ν	0.05	(0.001, 0.1)
Critical state	M	1.26	Fixed
	c	0.735	Fixed
	λ_c	0.0287	Fixed
	e_c^{ref}	0.78	Fixed
	ξ	0.7	Fixed
Yield surface	m	0.01	Fixed
Dilatancy	A_0'	0.626	(0.2, 1.4)
	n^d	2.5	(0.5, 4.0)
	n_g	0.9	(0.8, 1.0)
Kinematic hardening	n^b	3.5	(0.6, 2.5)
	h_0'	4.0	(1, 20)
	c_h	0.968	(0.3, 1.1)
Fabric-dilatancy	$z_{\max}$	15	(1, 20)
	c_z	2000	(500, 10000)
Memory surface	μ_0	4.08	(2, 10)
	u	3.63	(0.75, 4)
Semifluidized state	x	3.5	(1, 5)
	c_l	25	(10, 40)

needed. Critical state parameters, directly measured from experiments, were excluded from the optimization, and the parameter m (which controls the yield surface size) was fixed at 0.01. For comparison, a reference manual calibration for the Ottawa-F65 sand, as reported in Zeng et al. (2024), is also listed. All CDSS simulations assumed $K_0 = 0.4$.

3.3 *Cost function*

The overall error ϵ is a weighted sum of errors from all monotonic (ϵ^{mon}) and cyclic (ϵ^{cyc}) tests. Each is calculated as the average of the mean errors across different test types, where the mean errors are taken from each type of all corresponding tests. The error calculation based on comparison planes varies from test to test. In the same study, it was shown that, for the adopted model, SANISAND-MSf, the selection of comparison planes has a negligible effect on AC performance. As the database in this study includes only CD and CDSS tests, the overall error is given by:

$$\epsilon = \frac{1}{2}\epsilon^{CD} + \frac{1}{2}\epsilon^{CDSS} \tag{1}$$

where individual errors ϵ^{CD} and ϵ^{CDSS} are determined as follows:

$$\epsilon^{CD} = \frac{1}{n_{CD}} \sum_{i=1}^{n_{CD}} \left(\frac{1}{2}\epsilon_i^{\varepsilon_{ax} q} + \frac{1}{2}\epsilon_i^{\varepsilon_{ax} \varepsilon_v} \right) \tag{2}$$

$$\epsilon^{CDSS} = \frac{1}{n_{CDSS}} \sum_{i=1}^{n_{CDSS}} \left(\frac{1}{2}\epsilon_i^{Nr_u^{acc}} + \frac{1}{2}\epsilon_i^{N\gamma^{DA}} \right) \tag{3}$$

where n is the number of tests, $\epsilon_i^{\text{plane}}$ is the error for each test calculated on relevant comparison planes: axial strain vs. deviatoric stress ($\varepsilon_{ax} q$) and axial strain vs. volumetric strain ($\varepsilon_{ax} \varepsilon_v$) for CD tests; cycle number vs. end-of-cycle excess pore pressure ratio (Nr_u^{acc}) and cycle number vs. double amplitude shear strain ($N\gamma^{DA}$) for CDSS tests. For other plane combinations implemented in the ACT, the reader is referred to Machaček et al. (2022) and Machaček et al. (2025a).

3.4 *Calibration strategy*

The critical state parameters (M_c, λ_c, e_c^{ref}, ξ) were manually determined from CD tests. In the absence of triaxial extension tests, the parameter $c = M_e/M_c$ was set to 0.735. The yield surface size parameter m was fixed at 0.01. These six parameters remained fixed during optimization. All other model parameters were optimized within each bound using the ACT, following a two-stage calibration procedure:

- **Stage 1: based on monotonic test data**. Parameters primarily controlling monotonic behavior (G_0, ν, $A_0^{'}$, n^d, n^b, $h_0^{'}$, c_h) were calibrated using the 4 CD tests. Parameters influencing cyclic behavior were fixed at values obtained from Yang et al. (2022) since they do not impact the monotonic response. As only CD tests were used, the cost function was simplified to $\epsilon = \epsilon^{CD}$.
- **Stage 2: based on monotonic + cyclic test data**. The second stage focused on cyclic behavior, calibrating parameters $A_0^{'}$, n^d, n^b, $h_0^{'}$, c_h, n_g, $z_{\max}$, c_z, μ_0, u, x, and c_l based on the 18 CDSS tests and 4 CD tests. The five parameters inherited from the outcome of stage 1 ($A_0^{'}$, n^d, n^b, $h_0^{'}$, c_h) were re-optimized in stage 2 to enhance cyclic response flexibility, while the elasticity parameters (G_0, ν) remained fixed. CD tests were included to ensure that monotonic behavior was adequately captured. The cost function combined monotonic and cyclic errors equally, as in Eq. (1).

The two-stage calibration procedure was developed based on preliminary studies, which demonstrated advantages over simultaneous parameter calibration, particularly regarding the reproducibility and reliability of the calibrated parameters for simulating a system-level response. Moreover, by reducing the number of parameters to be optimized at once, the dimensionality of the optimization problem is reduced, thereby significantly improving computation time, convergence, and reproducibility of results, thereby mitigating the "curse of dimensionality".

3.5 *Calibration results*

The quality of optimized parameters is primarily assessed by the final cost function value, ϵ, where lower values indicate better agreement between simulations and experiments. Figure 2 shows the evolution of ϵ over five repeated runs for the first and second stages. All curves exhibit a clear drop and converge to lower values than their initial values. For the convergence rate of ϵ, which reflects optimization efficiency, the "monotonic" calibration rapidly reduces ϵ within 50 iterations and converges to a consistent final value. In contrast, the combined "monotonic + cyclic" calibration requires more iterations to achieve both substantial error reduction and stable convergence. This slower convergence stems from (a) higher parameter dimensionality, (b) incorporation of more diverse

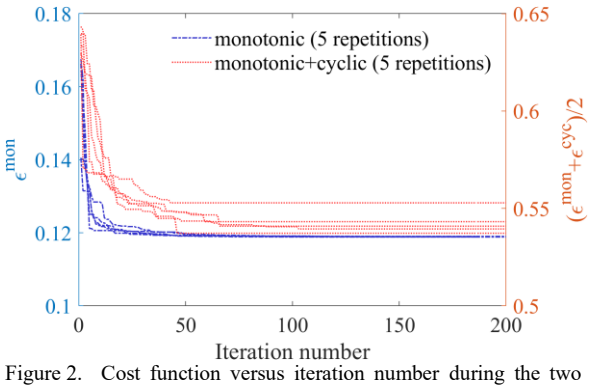

Figure 2. Cost function versus iteration number during the two optimization stages.

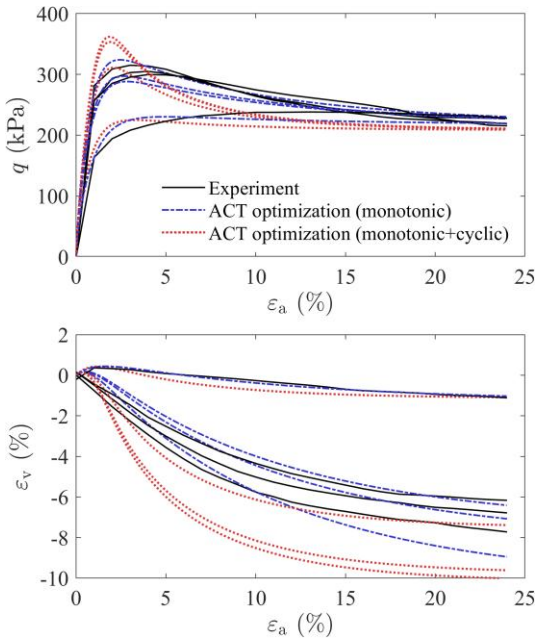

Figure 3. Comparison of experimental data from CD tests on Ottawa-F65 sand and simulation results using parameters from the first and second stages of optimization. Experiments from ElGhoraiby et al. (2020).

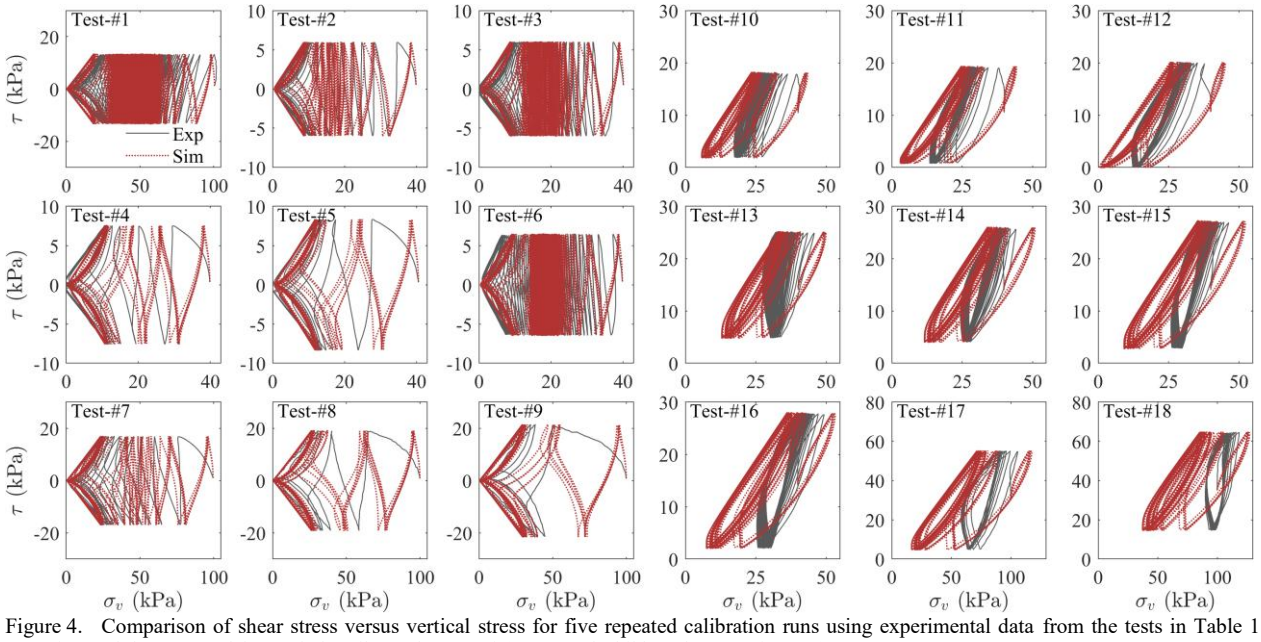

Figure 4. Comparison of shear stress versus vertical stress for five repeated calibration runs using experimental data from the tests in Table 1. Experimental data sourced from ElGhoraiby and Manzari (2021) and Lbibb and Manzari (2022).

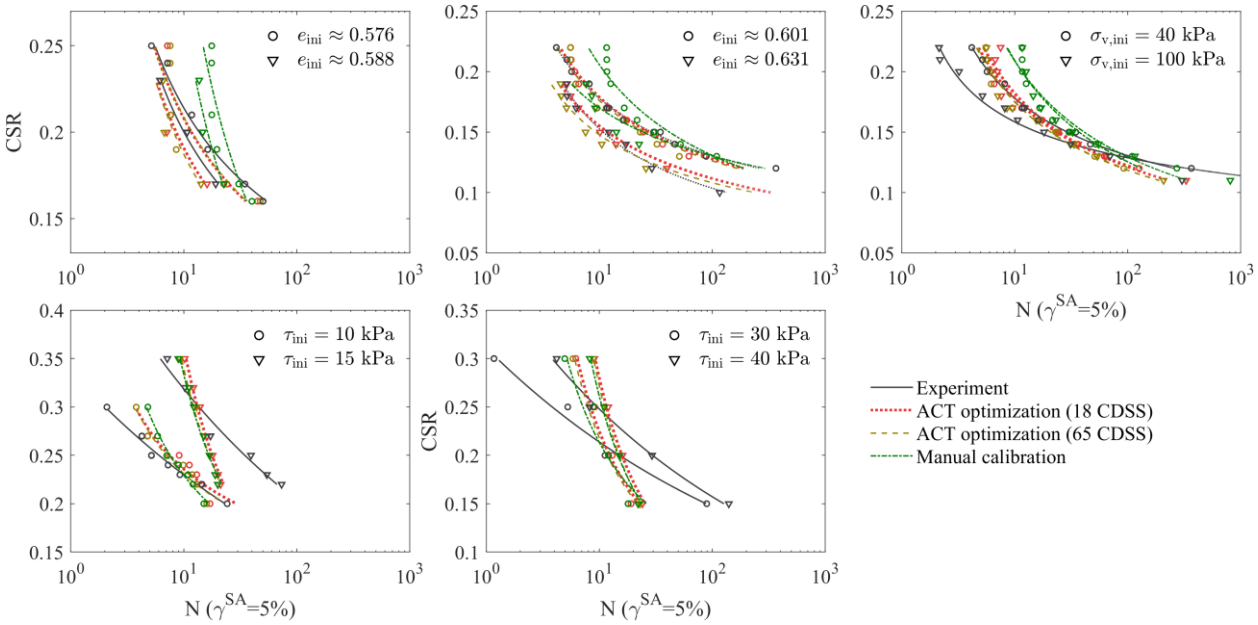

Figure 5. Summary of cyclic liquefaction resistance for experiments and calibration results considering the selected 18 or all 65 CDSS tests provided in ElGhoraiby and Manzari (2021) and Lbibb and Manzari (2022).

experimental data that impose additional constraints, and (c) the greater complexity of simulating cyclic behavior versus monotonic loading. Despite differences, both stages achieve efficient convergence of ϵ.

For stage 1, Figure 3 presents the calibration results from the four CD tests of one calibration run, color-coded in blue. Overall, the simulations agree reasonably well with the experimental data in both deviatoric stress and volumetric strain. It should be noted that parameters were further adjusted in stage 2, which calibrates both monotonic and cyclic tests. This combined calibration aims for an overall best fit for the behavior in CD and CDSS tests, somewhat potentially reducing accuracy in simulating CD tests, with respect to the peak shear stress and the corresponding volumetric strain, as shown in the red curves in Fig. 3.

In Stage 2, Figure 4 presents stress paths from 18 CDSS tests across five repetitions, demonstrating excellent agreement between simulations and experiments in effective stress reduction. To verify reproducibility, the automatic calibration was repeated five times. This reproducibility is crucial, as the stochastic nature of metaheuristic algorithms can produce varying outcomes. Nevertheless, the simulation results demonstrate the robustness of the algorithm and confirm the effectiveness of the chosen parameters.

So far, only 18 tests have been used for calibration, while the whole database includes 65 CDSS tests, raising the question of whether this subset sufficiently represents the full material behavior. To assess this, a representative parameter set, selected from the five repetitions based on the initial 18 tests, was used to simulate all 65 CDSS tests. The outcome, in terms of liquefaction resistance curves, is compared with experiments in

Figure 5. Simulations match experiments when the initial shear stress (τ_{ini}) is zero. Accuracy declines moderately as τ_{ini} increases to a non-zero value, with larger deviations across CSRs. This limitation stems from the S-MSf model's current inability to fully capture liquefaction behavior under varying initial shear stresses, a shortcoming addressed in a recent enhancement (Reyes et al., 2025). Even with this limitation, the 18 selected tests with diverse initial conditions generally capture soil behavior within the S-MSf model's capabilities. Additionally, simulation results using all 65 tests for ACT optimization and manual calibration from Zeng et al. (2024) are also provided as a reference. The comparison of the ACT optimization results, derived from 18 and 65 CDSS tests, respectively, reveals a high degree of similarity and consistent agreement with experimental data. This finding demonstrates that a well-selected subset of tests covering the necessary range of experimental conditions can serve as an efficient and accurate basis for calibration, avoiding the more time-intensive process required for the entire data set. A comparison of the simulation results obtained with parameters from manual calibration indicates better performance of AC parameters, especially noticeable for zero τ_{ini} cases, where manually calibrated parameters prioritize initial liquefaction.

4 APPLICATION TO LIQUEFIABLE SLOPE

To further evaluate the effectiveness of numgeo-ACT with the S-MSf model and to demonstrate the robustness of AC parameters for system-level simulation in boundary value problems (BVPs), a centrifuge test conducted as part of the LEAP project was simulated in OpenSees using the optimized model parameters.

4.1 *Main features*

For the back-calculation, the centrifuge test NCU-3 from LEAP-2017 (Hung et al., 2018) was chosen. The centrifuge test features a submerged slope of medium-dense Ottawa-F65 sand subjected to base excitation. The test evaluates the undrained dynamic response and the performance of the S-MSf model. In prototype scale, the model represents a 20 m long, 4 m deep submerged slope with an inclination of about 5 degrees. The deposit has an initial relative density of D_r=64% corresponding to a void ratio e=0.607. The centrifuge scaling factor was 26.

The numerical model was developed at prototype scale under plane-strain conditions, following the settings reported in Machaček et al. (2025a). The soil domain was discretized using stabilized four-node quadrilateral elements with reduced integration, where solid displacement and pore pressure were treated as nodal degrees of freedom. The mesh and boundary conditions are plotted in Fig. 6, with a control point AH4 for recording horizontal acceleration and P2 for porewater pressure.

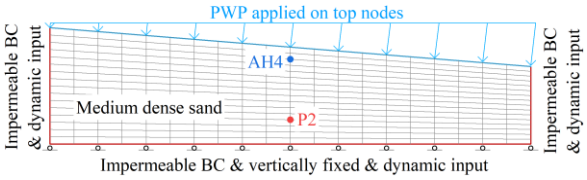

Figure 6. Spatial discretization and boundary conditions during dynamic stage.

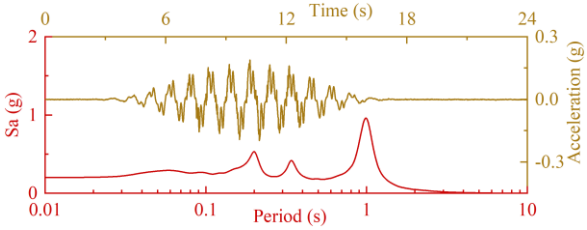

Figure 7. Achieved motion's time history and spectral acceleration response (Sa).

The centrifuge model was subjected to a base excitation in the form of a ramped sine signal with a dominant frequency of 1 Hz, featuring build-up and decay phases corresponding to increasing and decreasing acceleration amplitudes. Figure 7 shows the achieved acceleration signal recorded at the base of the centrifuge test. For the numerical simulation, a linear baseline correction was applied to ensure zero velocity before and after shaking. A band-pass Butterworth filter (0.2–25 Hz) was used to reduce noise from the centrifuge shaker system. The simulation procedure consisted of two primary stages:

- **Self-weight analysis**, which starts from an equilibrium substage under self-weight, utilizing only the nonlinear elastic component of the S-MSf model, and then switches to the full elastoplastic formulation to achieve equilibrium again. The degrees of freedom for pore water pressure at the surface nodes were initialized with the corresponding hydrostatic water pressure, applied as a normal pressure at the start of the self-weight stage.
- **Dynamic excitation**, by synchronously exciting the base and lateral sides of the model via a force signal obtained by multiplying the velocity time history of the input motion by the dashpot coefficients, determined from the mass density, shear wave velocity, and base length. Rayleigh damping was set to 1% at a center frequency of 1 Hz to reduce simulation noise, and a constant timestep of 0.001 s was used during the dynamic stage.

4.2 *Simulation results*

Simulations of the liquefiable sand slope were performed using either (i) the five sets of parameters from repeated ACT optimizations discussed in Section 3 or (ii) the reference parameters obtained by manual calibration. Figure 8(a) shows the spectral acceleration (Sa) at control point AH4. Most results

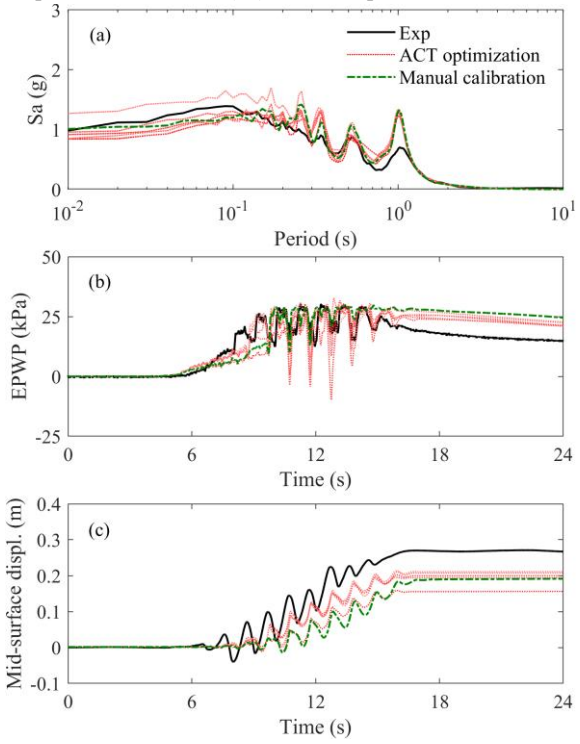

Figure 8. Experimental and simulation results of (a) spectral acceleration at AH4, (b) excess porewater pressure at P2, and (c) mid-surface displacement.

using ACT-optimized parameters align well with the experimental data across a broad range of periods, while the results using manually calibrated parameters fall within the range of those from AC.

Figure 8(b) shows the excess pore water pressure (EPWP) time histories at control point P2. In all simulations, the EPWP builds up and reaches a plateau comparable to experimental data, indicating the onset of cyclic liquefaction. All simulations using parameters from five runs of ACT exhibit consistent behavior, and the results are generally comparable to those from both experiments and those obtained using manually calibrated parameters.

Figure 8(c) compares the mid-surface displacement time histories calculated using the five parameter sets from AC, alongside experimental data and results from manual calibration. The simulations capture both the accumulation trend and oscillations, especially the final displacement after shaking. The five runs show consistent convergence, indicating good stability. Although the mid-surface point reflects only a localized response and is sensitive to uncertainties, it is still well captured by the simulations.

5 CONCLUSION

This study presents the development and application of numgeo-ACT (numgeo Automatic Calibration Tool) for advanced soil constitutive models under both monotonic and cyclic loading conditions. The SANISAND-MSf model was chosen for the investigation as a representative of advanced constitutive models capable of simulating cyclic liquefaction, among other things. The main findings of this research are as follows:

- **Enhanced Calibration Process:** A two-stage calibration procedure was adopted, streamlining the calibration process and enabling effective parameter optimization for both monotonic and cyclic loading. This approach successfully reduced the problem dimensionality, thereby improving computational efficiency, convergence behavior, and reproducibility.
- **Reproducibility and Stability**: The automatically calibrated parameters were evaluated through CDSS and centrifuge test simulations of a liquefiable sand slope subjected to base excitations. In both cases, good agreements with experiments and those from expert manual calibration were achieved. Multiple calibration runs yielded consistent results, demonstrating the robustness and reliability of the numgeo-ACT approach for geotechnical applications.
- **Knowledge requirement**: While automatic calibration significantly enhances the efficiency and accessibility of constitutive model calibration, it does not replace the need for a clear understanding of the model's general features, capabilities, and limitations to ensure its proper use and interpretation. Nonetheless, numgeo-ACT proves to be a valuable tool in geotechnical engineering, offering an efficient and reliable solution for calibrating complex soil models.

6 ACKNOWLEDGEMENTS

M. Taiebat and S. Zeng acknowledge partial support from the Natural Science and Engineering Research Council of Canada (NSERC) and BGC Engineering.

7 REFERENCES

Barrero, A.R., Taiebat, M., and Dafalias, Y.F. 2020. Modeling cyclic shearing of sands in semifluidized regime. *International Journal for Numerical and Analytical Methods in Geomechanics*, 44(3), 371–388.

Brosz, F., Machaček, J., and Zachert, H. 2023. Automatic parameter calibration of two sophisticated soil models based on monotonic and cyclic tests on sand, *in: Proceedings 10th NUMGE 2023*, Imperial College, London.

Corti, R., Diambra, A., Wood, D.M., Escribano, D.E., and Nash, D.F.T. 2016. Memory surface hardening model for granular soils under repeated loading conditions. *Journal of Engineering Mechanics*. 142 (12), 04016102.

Dafalias, Y.F., and Manzari, M.T. 2004. Simple plasticity sand model accounting for fabric change effects. *Journal of Engineering Mechanics*, 130, 622–634.

ElGhoraiby, M.A., Park, H., and Manzari, M.T. 2020. Stress-strain behavior and liquefaction strength characteristics of Ottawa F65 sand. *Soil Dynamics and Earthquake Engineering*, 138, 106292.

ElGhoraiby, M., and Manzari, M. 2021. LEAP-2020: Cyclic triaxial a nd direct simple shear tests performed at GWU. *Designsafe*. [Online] Available at: https://www.designsafe-ci.org/data/browse r/public/designsafe.storage.published/PRJ-2557

Ghofrani, A. 2018. Development of numerical tools for the evaluation of pile response to laterally spreading soil. *Ph.D. thesis*, University of Washington.

Hung, W.Y., Ting-Wei, L., and Hu, L.M. 2018. NCU1, NCU2, NCU3 - National Central University experiments, in PRJ-1843: LEAP-UCD-2017. [Online] Available by doi:10.17603/DS2VH72.

Kutter, B.L., Manzari, M.T., and Zeghal, M. (Eds.). 2020. Model Tests and Numerical Simulations of Liquefaction and Lateral Spreading: LEAP-UCD-2017. *Springer International Publishing Cham*.

Lbibb, S., and Manzari, M., 2022. LEAP-2022 - effects of overburden stress, relative density, and static shear stress on cyclic strength o f Ottawa F65 sand. *Designsafe*. [Online] Available at: https:// www.designsafe-ci.org/data/browser/public/designsafe.storage.p ublished/PRJ-3484

Liu, H.Y., Abell, J.A., Diambra, A. and Pisanó, F. 2019. Modeling the cyclic ratcheting of sands through memory-enhanced bounding surface plasticity. *Géotechnique*, 69(9), 783–800.

Machaček, J., Staubach, P., Tavera, C.E.G., Wichtmann, T., and Zachert, H. 2022. On the automatic parameter calibration of a hypoplastic soil model. *Acta Geotechnica*, 17(11), 5253-5273.

Machaček, J., Siegel, S., Staubach, P., and Zachert, H. 2023. Automatic parameter calibration of two advanced constitutive models, *in: Challenges and Innovations in Geomechanics. Springer International Publishing, Cham*, 288, pp. 110–117.

Machaček, J., Zeng, S., and Taiebat, M. 2025a. Enhancing accuracy and efficiency in cyclic liquefaction modeling: An automatic calibration framework for advanced constitutive models. *Computers and Geotechnics*, 183, 107208.

Machaček, J., Siegel, S., and Zachert, H. 2025b. DEEM — differential evolution with Elitism and Multi-populations. *Swarm and Evolutionary Computation*, 92, 101818.

Reyes, A., Taiebat, M., and Dafalias, Y.F. 2025. Modification of SANISAND-MSf Model for Simulation of Undrained Cyclic Shearing under Nonzero Mean Shear Stress. *Journal of Geotechnical and Geoenvironmental Engineering*, *151*(7), p.04025051.

Sloan, S.W., Abbo, A.J., and Sheng, D. 2001. Refined explicit integration of elastoplastic models with automatic error control. *Engineering Computations*, 18, 121–194.

Yang, M., Taiebat, M., and Dafalias, Y.F. 2022. SANISAND-MSf: A sand plasticity model with memory surface and semifluidised state. *Géotechnique*, 72, 227–246.

Zeng, S., Reyes, A., and Taiebat, M. 2024. Modeling cyclic liquefaction and system response of a sheet-pile supported liquefiable deposit: Insights from LEAP-2022. *Soil Dynamics and Earthquake Engineering*, 179, 108548.